
Article:
Al-Khafaji, A, Wilson, M orcid.org/0000-0002-1058-2003, Neville, A orcid.org/0000-0002-6479-1871 et al. (1 more author) (2019) Pore-Scale Displacement Efficiency during Different Salinity Water Flooding in Hydrophilic and Hydrophobic Microstructures. Energy and Fuels, 33 (5). pp. 3859-3870. ISSN 0887-0624

https://doi.org/10.1021/acs.energyfuels.8b04295

Pore-Scale Displacement Efficiency during Different Salinity Water Flooding in Hydrophilic and Hydrophobic Microstructures

Arije Al-Khafaji[1], Mark Wilson[2], Anne Neville[2], Dongsheng Wen[3,1*]

[1] Chemical and Process Engineering Department, University of Leeds, Leeds, UK.

[2] Mechanical Engineering Department, University of Leeds, Leeds, UK.

[3] School of Aeronautic Science and Engineering, Beihang University, Beijing, 100191, China.

E-mail: D.Wen@leeds.ac.uk

Abstract

Previous macroscopic core flooding tests have shown that injecting low salinity water improves oil recovery in sandstone and carbonate reservoirs through wettability alteration. However, consistent mechanistic clarification of the underlying physicochemical mechanisms involved in oil wettability at the pore-scale level is not fully understood. In this work, a microfluidic approach is used to provide in-situ visualization of oil-brine flow to give an indication of the micro-mechanisms affecting oil sweep efficiency. The potential of enhancing oil recovery by low-salinity flooding at the microscale is also investigated, which would help in predicting a reservoir's performance before committing to production processes at a large field scale. Two types of crude oils with various acid numbers were used, and hydrophilic and hydrophobic physical microstructures were used to mimic sandstones and carbonates. The results revealed a reduction by 7-10% in the residual oil for the water-wet microstructure when the seawater was diluted twice from its original concentration, apparently due to a decrease in the attractive forces. There is no change in the recovery factor for the oil-wet micromodel for the two kinds of crude oils examined. Tertiary low-salinity flooding did not show any effect on the initial wetting state of the hydrophobic surface, rendering it with a strongly oil-wet condition. It is also observed that flow dynamics of the two microstructures examined are different, as the snap-off-coalesce phenomenon

dominants the flow in the water-wet system, while oil moved by a piston-like displacement with a stable or irregular front in the hydrophobic system. In contrast to some of the published macroscopic results, our pore-scale displacement shows that low salinity flooding seems to be an unsuitable choice for enhanced oil recovery for strongly oil-wet reservoirs.

Keywords: low salinity, enhanced oil recovery, wettability, pore-scale displacement, carbonates

1. Introduction

Enhanced oil recovery (EOR) techniques have a long history, but much development has taken place in the last two decades. Recently, smart water has been considered as an emerging and economical EOR technique for extracting the residual oil and increasing the recovery factor of the hydrocarbon reservoirs. In the literature, there is a general agreement that reducing the salinity of water below 5000 ppm revealed positive results for sandstone reservoirs by shifting rock wettability from mixed-wet to more water-wet conditions [1-8]. However, some of these studies showed that low-salinity water flooding is not sufficient for carbonate reservoirs and its effect has only been detected for sandstone reservoirs with a high clay content [1,9]. In recent years, a number of authors found that injecting low-salinity water could improve oil recovery in carbonate reservoirs [10,11]. Despite this interest, the feasibility of low-salinity flooding in carbonates is still controversial due to a poor understanding of the detailed mechanisms behind the process.

Wettability alteration to a favorable wet condition, detected indirectly through changes in relative permeability or capillary pressure [3], is the most plausible mechanism, significantly affecting EOR during low salinity water flooding [4,11-18]. However, there is no universal agreement on the physicochemical mechanisms behind this alteration. This could be due to the fact that most of the

macroscopic techniques exhibit some restrictions on providing in-situ microscopic detail of the physicochemical interactions that take place between interfaces. This leads to a lack of reliable predictions of reservoirs' performance under low-salinity flooding, calling for more efficient methods for assessing wettability at the scale of pore surface heterogeneities. Microfluidics is an ideal technique for this purpose and has been used previously as a diagnostic platform in biological and chemical processes [19,20]. In recent times, microfluidic technology has gained a wider acceptance for use in the oil and gas sector. For instance, Sieben et al. [21] used a microfluidic apparatus as a rapid method for measuring the fractional amounts of saturates, aromatics, resins, and asphaltenes in crude oil. Lin et al. [22] utilized a microfluidic T-junction device consisting of a collision chamber for in-situ observation of coalescence rate in different monodisperse water-in-oil emulsions. Such a device was also used to study the fundamental aspects of gas flotation by evaluating the impact of salinity, oil, and gas compositions, as well as oil droplet size on oil attachment efficiency through spreading of oil over the gas bubbles surfaces [23].

A number of researchers have sought to evaluate the effectiveness of different flood processes to enhance oil recovery by using an optical microfluidic apparatus. These include water flooding in different periodic and random pore networks [24,25], multiphase flow using non-Newtonian fluids with various rheological properties [26], foam flooding [27,28], multiphase flow with synergetic nanoparticles and surfactants in macroemulsions [29], polymer flooding using shear-thinning fluids and hydrophilic micromodels with varying grain sizes [30], and multiphase flow using hydrophilic silica nanoparticles suspended in seawater (SW) [31].

More recently, there has been growing interest to evaluate the effectiveness of low-salinity water flooding to enhance oil recovery in sandstones at the pore-scale. In 2013, Emadi and Soharbi [32] conducted visualization experiments of fluid movement in a homogenous water-wet micromodel at reservoir conditions. They found that when high-salinity water was replaced by low-salinity solution,

microdispersions (water-in-oil emulsion) at oil/water interfaces were formed, which was considered as an underlying mechanism affecting the fluid redistribution and sweep efficiency. Another study by Barnaji et al. [33] on the potential of low salinity for EOR in sandstones suggested that low-salinity water flooding did not show any improvement in the oil recovery for a non-coated pore network, i.e., with no clay minerals. Amirian et al. [34], however, showed different results to those of Barnaji et al. [33] that no correlation was found between the presence of clay minerals and the potential of low-salinity water flooding for EOR. This raises ambiguity regarding the effect of clay minerals, and thus further studies are needed to fill the general gap in our knowledge. A very recent study by Fredriksen et al. [35], in which they examined the mobilization of oil at a microscale using silicon-wafer micromodels, demonstrated that osmosis and diffusion of water molecules driven by salinity contrasts represented the main pore-scale mechanisms responsible for oil mobilization during low-salinity flooding.

From the aforementioned literature, it is clear that the microfluidic technique has been used by many researchers to evaluate the performance of different displacing fluids to improve oil recovery in silicate-glass micromodels, but there is no consensus on the underlying micromechanisms affecting oil recovery during low-salinity flooding. On the other hand, most of the previous pore-scale studies up to now have been conducted on the strongly water-wet microstructures, representing sandstone reservoirs. However, too little attention has been paid to assess the pore-scale displacement efficiency in an oil-wet system to resemble carbonates, which prevail in most of the world's oil reserves (>60%) [36]. It should, however, be important to emphasize here that most of the hydrocarbon reservoirs are initially water-wet due to the hypothesis that the reservoir was originally occupied by water before the migration of the hydrocarbon and then rock surfaces turn into more oil-wet as a result of the presence of polar organic compounds in crude oil, which help to diffuse a thin film of interstitial water; thereby, oil is attracted to the rock surfaces rendering it to oil-wet [37].

In this work, we provide surrogate rock pore structure with full visualization of fluid movement to understand the complexities of the various interfacial phenomena governing surface wetting of crude oil on carbonates and sandstones in a brine environment, giving an indication of the underlying mechanisms affecting oil sweep efficiency at the microscale. Silicon glass and polymer-coated physical pore networks were used to mimic the hydrophilic (sandstones) and hydrophobic (carbonates) surfaces, respectively. Two kinds of crude oils with various chemical properties were used for the drainage process, while synthetic seawater and different diluted versions of seawater were used for the imbibition displacement. The dynamics of displacement of various saline solutions in the water-wet and oil-wet systems are critically compared. The potential of low-salinity water flooding to improve the microscopic sweeping efficiency and the associated wettability effects are visually evaluated.

2. Materials and Methods

2.1 Microfluidic chips

Two-dimensional silicon glass and polymer-coated chips (45 × 15 mm^2; length × width) from Micronit were used to mimic natural hydrophilic and hydrophobic surfaces. The chip has a physical pore network to resemble a real physical rock pattern. The chip is designed by randomly engraving the rock shape structures onto a glass plate by laser. Such kind of random placement gives throats in the channels that go between the rocks. The chip has a total internal volume of 5.7 µl, a mean channel width of 50 µm, and a mean channel height of 20 µm. The average porosity and permeability of the two-dimensional microstructure are 0.57 and 2.5 Darcy, respectively. Porosity is estimated by using image analysis technique by dividing the number of pixels, which belongs to the pore space with the total number of pixels of a given image, while permeability is calculated by measuring the differential pressure across the chip and applying Darcy's law [24]. Figure 1 illustrates the schematic diagram and microscopic images of the physical pore network considered in this study.

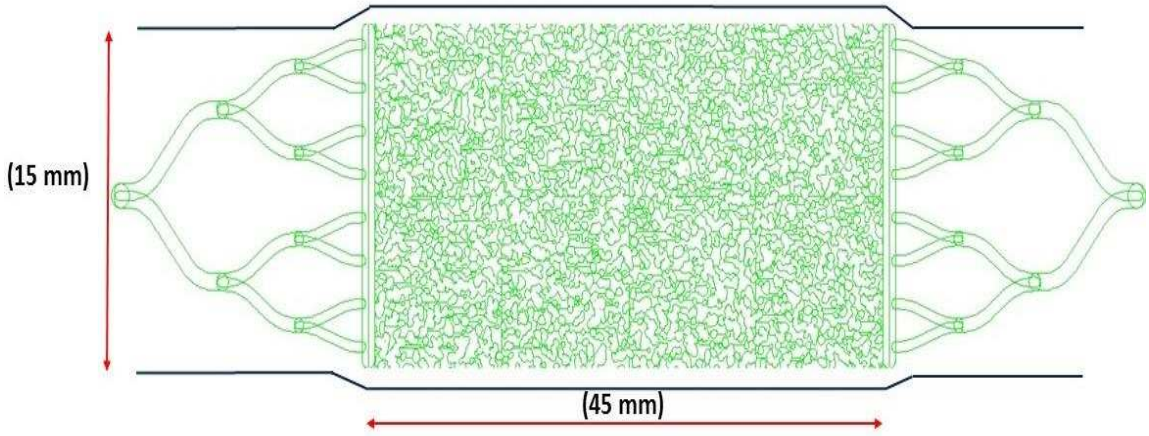

(A)

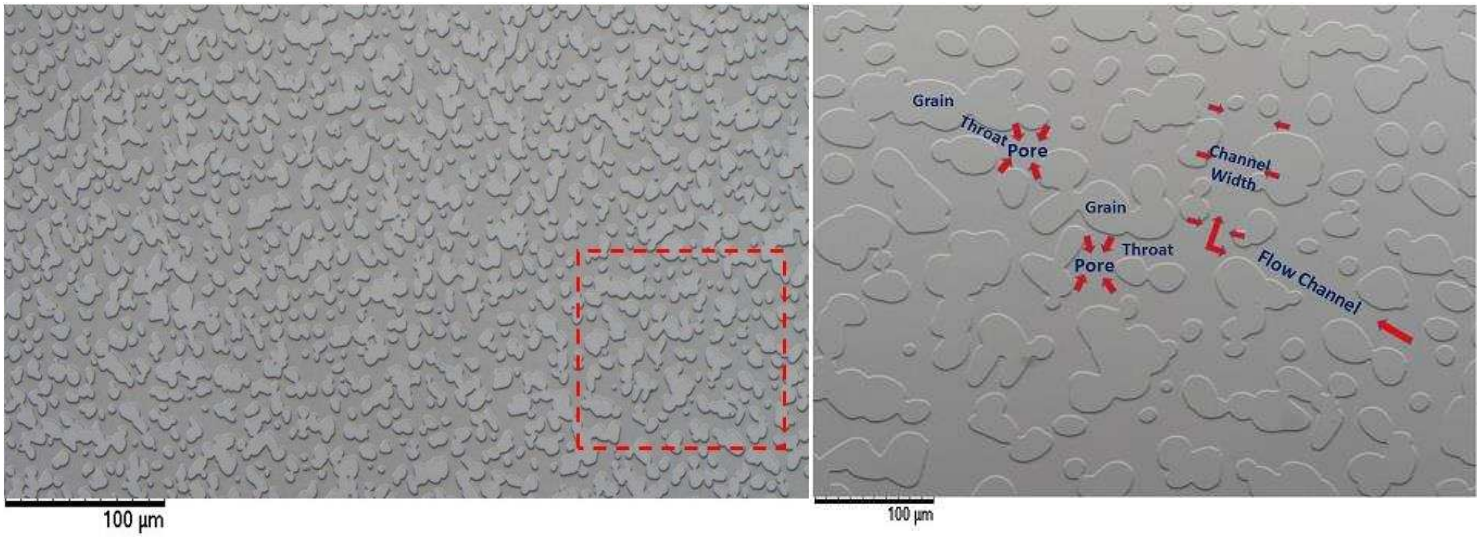

(B) **(C)**

Figure 1. (A) Schematic diagram of the physical structure (pores and throats are displayed as channels in green and grains in white). (B) Full-length image shows the geometry of the physical network. (C) Magnified section from the red square in (B) shows the pore-throat distribution and flow channels in the network.

2.2 Brines

The same synthetic brines used in our previous work [37] were also utilized in this study. Synthetic seawater (SW) and artificial formation water (FW) were used as the high salinity brines. All brines were prepared in the lab by mixing deionized water (Milli-Q, a resistivity of >18.2 MΩ.cm) with reagent grade salts (Merck, Sigma-Aldrich, a purity grade of > 99%). The artificial low salinity (LS) solutions were made by diluting the prepared seawater with different proportions of deionized water, see Table 1. The physical properties of all prepared brines were characterized, and the details are given previously [38].

Table 1. The composition of high salinity and low salinity brines

Salts	FW	SW	2dSW	5dSW	10dSW	20dSW	50dSW
NaCl	124.50	26.50	13.25	5.30	2.65	1.33	0.53
Na_2SO_4	0.43	4.10	2.05	0.82	0.41	0.20	0.08
$CaCl_2.2H_2O$	57.79	1.54	0.77	0.31	0.15	0.08	0.03
$MgCl_2.6H_2O$	16.87	11.41	5.70	2.28	1.14	0.57	0.23
$NaHCO_3$	0.40	0.11	0.05	0.02	0.01	0.01	0.00
TDS (g/L)	200.00	43.65	21.82	8.73	4.37	2.18	0.87
Salt concentration (ppm)	200000	43650	21828	8731	4366	2183	873
pH	6.70	7.96	7.58	7.34	7.24	7.15	7.01
IFT Oil A*	35.00	31.80	30.50	29.54	28.73	27.21	25.66
IFT Oil B*	37.70	34.60	33.71	32.80	31.70	31.00	30.60

* Interfacial tension for oil/brine system (mN/m), measured by CAM 200-KSV.

2.3 Crude oil

Two types of dead crude oils were supplied by Shell from an oil field in the North Sea. A Malvern Bohlin Rheometer and Micromeritics Acupyc-1330 were used to measure viscosity and density, respectively. The bulk composition of oils was analyzed by SARA fractionation technique. The physicochemical properties of the crude oils are listed in Table 2.

Table 2. Physicochemical properties of crude oils

Specification	Crude Oil A	Crude Oil B
Specific gravity at 25 ℃, gm/cm ^{3}	0.84	0.83
℃API	38.00	39.5
Dynamic viscosity at 20 ℃, cp	7.40	5.50
Dynamic viscosity at 50 ℃, cp	4.52	2.94
Total acid number (TAN), mg KOH/g	0.46	0.25
Composition (wt. %) @25 ℃		
Saturates	64.53	73.70
Aromatics	28.81	22.75
Resin	6.19	3.34
Asphaltenes	0.47	0.21
Elemental analysis (wt. %) @ 25 ℃		
Nitrogen	0.88	1.14
Sulphur	0.19	0
Oxygen	5.12	2.2

2.4 Experimental Procedure

In this work, the microfluidic apparatus was used to visualize oil displacement in porous media during secondary and tertiary flooding, as shown in Figure 2. The system consisted of a microfluidic solid casing to hold the chip with inlet and outlet ports, high pressure syringe pump (Nexus 6000) with a minimum flowrate of 0.0001 µl/min, a polyetheretherktone tubing (OD= 1/16″, IDEX) to join the inlet of the chip to the pump, a controlling valve to control the direction of flow, and pressure transducers. A high magnification microscope (Olympus SZX16-ILLT) was used to visualize the chip, which was outfitted with a digital camera (5 M pixel, Colour USP3 Vision, Sony Pregius IMX250, Canada) to capture digital images when the fluids flow along the pore channels. The images were recorded every 20 seconds by Point Grey Fly Cap 2 software.

To perform the experiments, the microfluidic physical chip was put into the casing and an Isopropyl alcohol, IPA (Sigma-Aldrich, purity grade of > 99%) was

first flushed through the chip to remove trapped air bubbles, followed by rinsing with a sufficient amount of Milli-Q water. Afterward, the clean pore network was saturated with a super saline solution (200000 ppm), representing formation water in the real reservoirs. Next, 10 pore volumes of dead crude oil were injected at a steady flowrate of 50 μl/hr to displace formation water and establish initial water saturation (S_{wi}). The saturated microchip was then left for about 24 hours to attain the adsorption equilibrium conditions. To increase the distinction between high- and low-salinity solutions during the pore-scale displacement, a red tracer dye (Rhodamine B base, Sigma-Aldrich) was mixed with the injected low saline solutions. Seawater was then pumped in a secondary mode recovery, whereas tertiary mode recovery was performed by sequentially injecting different diluted versions of seawater through the microphysical chip. The low injection rate of 5 μl/hr was used in all cycles of the injection, representing the typical pore velocity (1 m/day) in real reservoir water flooding. After oil production is stopped, the injection rate was increased to 10 and 15 μl/hr for each cycle of brine injection to ensure that the remaining oil saturation was reached, and no more oil was visibly removed with the higher flow rate. For each stage of the displacement, the saline solution was continuously flooded for 6-12 hours. Optical images for fluid distribution were recorded at different stages of secondary and tertiary flooding. The microscale displacements were conducted at ambient temperature (23°C) and atmospheric pressure. For data reliability, the flooding tests were repeated two times for both microstructures examined.

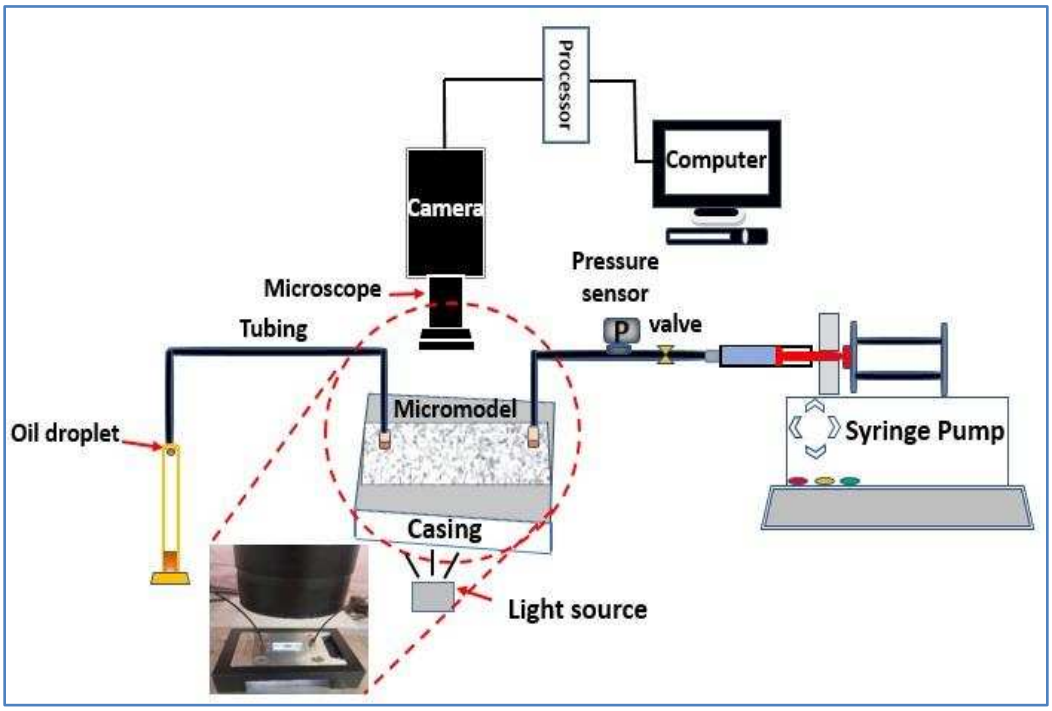

Figure 2. Schematic diagram of microfluidic system used in the experiments.

2.5 Image Analysis

A set of digital images acquired during the displacement process were quantitatively analyzed using image processing software FIJI to evaluate the quantity of oil recovered after each stage of brine injection. The digital images were first segmented to distinguish between phases. The oil-filled pore spaces were then identified by thresholding of its pixels' intensity, Figure 3B, and the oil area was represented completely by red, while non-oil area appeared as black. After that, the images were binarized and the pixels of oil were counted (see Figure 3C). The microscopic sweeping efficiency during brine flooding was determined by the following equation [39]:

$$E_m = \frac{1 - S_{or} - S_{wir}}{1 - S_{wir}}$$

where, S_{or} is remaining oil saturation upon exposure to the saline solution and S_{wir} is irreducible water saturation, i.e., the percentage determined when the chip was saturated with oil and before starting the displacement process.

The dynamic contact angle during brine imbibition was also assessed by using FIJI contact angle plugin. The best-fit analysis automatically detects the contact angle at the intersection of the tangent line. Contact angles (40) were measured for each type of the micromodel examined by a random selection of different locations on the network. Each measurement was repeated, and the accuracy of the measured contact angle is reported to be ± 2°. The minimum, mean, and maximum contact angles for the hydrophilic system were determined to be 20°, 35°, and 49°, respectively. For the hydrophobic system, the measured contact angles ranging from 102° to 140° with a mean value of 115°.

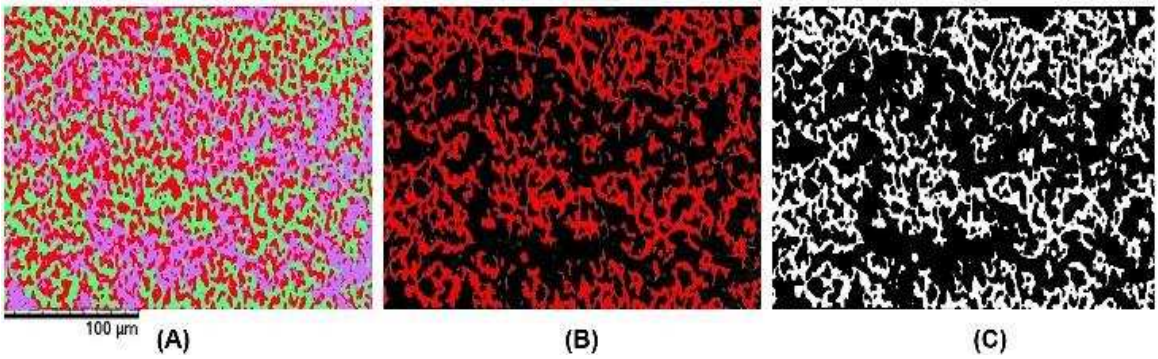

Figure 3. Typical example of the image analysis procedure by FIJI for determining the residual oil saturation after brine flooding. (A) Segmented image with red for grains, light green for oil, and pink for brine. (B) Image after thresholding to distinguish between oil phase in red and background in black. (C) Binary image with oil phase in white.

3. Results and Discussion

3.1 Effect of salinity on the pore-scale displacement efficiency in a hydrophilic network

Table 3 summarizes the observed results from the series of pore-scale displacement of the hydrophilic and hydrophobic microstructures. The initial oil saturation was almost the same (0.88-0.89) after drainage displacement for the water-wet micromodel saturated with crude oils A and B, respectively. The residual oil saturation at the end of secondary flooding by seawater (imbibition) was determined to be 0.37 and 0.23, i.e. 57.9% of the oil in the system were recoverable in the pore network saturated with crude oil A, but with a significant displacement (74%) for that saturated with crude oil B, having less polar organic components (acid number= 0.25 mg KOH/g). For each oil/brine system, the flooding tests were repeated, and the observed oil saturation trend was almost the same with a small variation of about 3%. The discrepancy in the microscopic sweeping efficiency could be attributed to the difference in the oil composition, represented by the concentration of active polar components. Polar compounds composed of heteroatoms such as oxygen, nitrogen, and sulphur, which were generally found in the resin and asphaltene fractions of crude oil [40]. The oxygen compounds are mainly carboxylic acids (-COOH), but also include phenolic acids [37,41]. Carboxylic acids are interfacially active due to their polarity and hydrophilicity, and even quantities in the lower range could have an influence on the interfacial activity [42]. The quantity of petroleum acids is characterized by the total acid number (TAN), equivalent to the milligrams of KOH required to neutralise the acidity of 1g of oil [42]. Therefore, if we consider crude oil A with a high polar content (O=5.12 wt.%, TAN= 0.46 mg KOH/g) and with the presence of high saline solution, we can expect that the acidic components will tightly bind to the divalent cations (Ca^{2+} and Mg^{2+}) of seawater, resulting in less desorption efficiency for crude oil A compared to crude oil B. Farooq et al. [43] also found that the high concentration of divalent ions resulted in less desorption efficiency due to the complex formation between Ca^{2+} and dissociated asphaltene groups. On the other hand, injection seawater which has a high concentration of monovalent cations (Na^{+}), could lead to the

replacement of the divalent cations that are bonded to the acidic polar components by these monovalent cations, helping to detach some of the polar components from the surface and improve the displacement efficiency.

A typical example of the segmented images of water-wet micromodel, showing oil distribution after high- and low-salinity water flooding is illustrated in Figure 4. The overall pressure drop across the micromodel was also measured, as shown in Figure 5. It is clear that a considerable increase in the maximum pressure difference was observed, particularly at the earlier stage of seawater flooding, suggesting a high capillary pressure and a strong resistance to the water flow and therefore a higher viscous pressure drop is required to overcome the critical capillary entry pressure. Afterward, the pressure drop was decreased and was relatively stable as a result of oil production and an increase in the relative permeability of water.

Table 3. Summary of micromodel experiments

Micromodel type	Crude oil	Wettability	Initial oil saturation (S_{oi})	Residual oil saturation (S_{or}) at secondary mode	Residual oil saturation (S_{or}) at tertiary mode	Oil recovery enhancement (%)
silicon-glass	A	water-wet	0.88	0.37	0.30 - 2dSW 0.29 - 5dSW	8
silicon-glass	B	water-wet	0.89	0.23	0.14 - 2dSW	10
polymer-coated	A	oil-wet	0.87	0.50	0.50	0
polymer-coated	B	oil-wet	0.84	0.47	0.46 - 2dSW	1

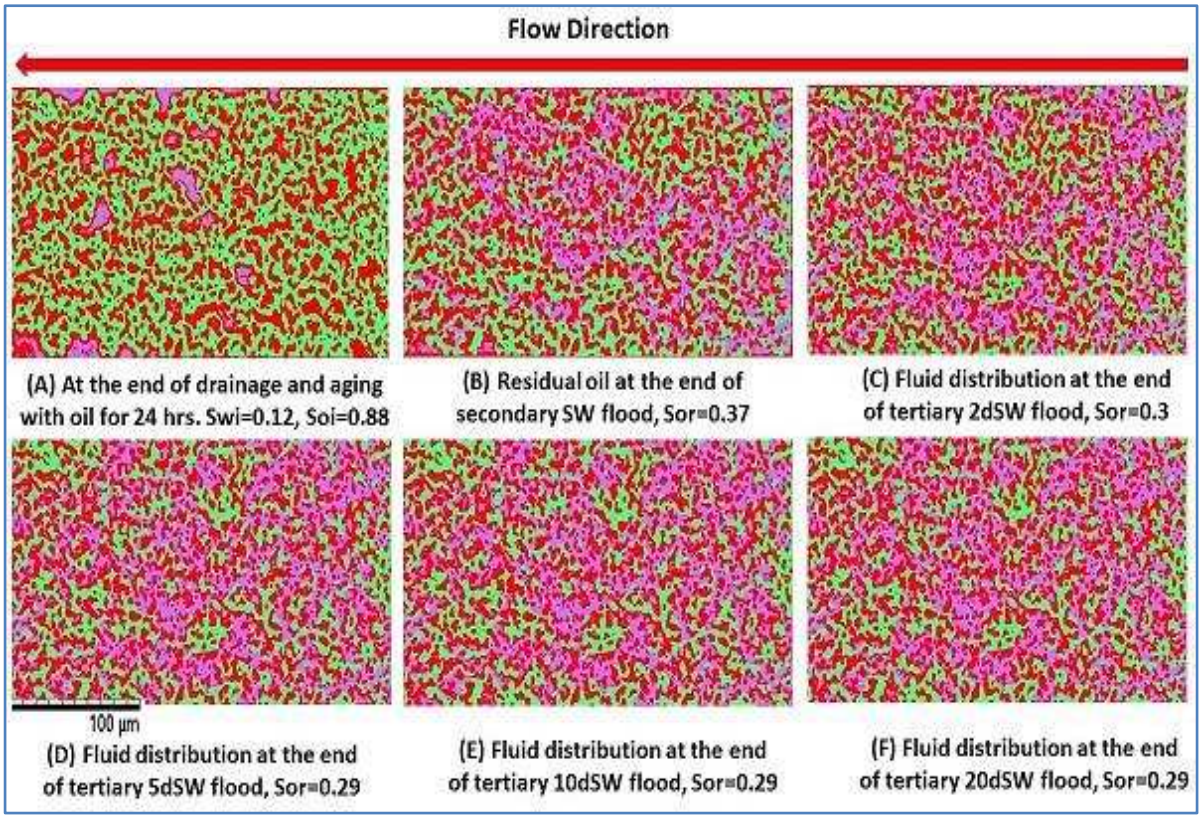

Figure 4. Micromodel images after secondary and tertiary flooding in a hydrophilic surface saturated with crude oil A. Red: grains, green: oil, purple: brine.

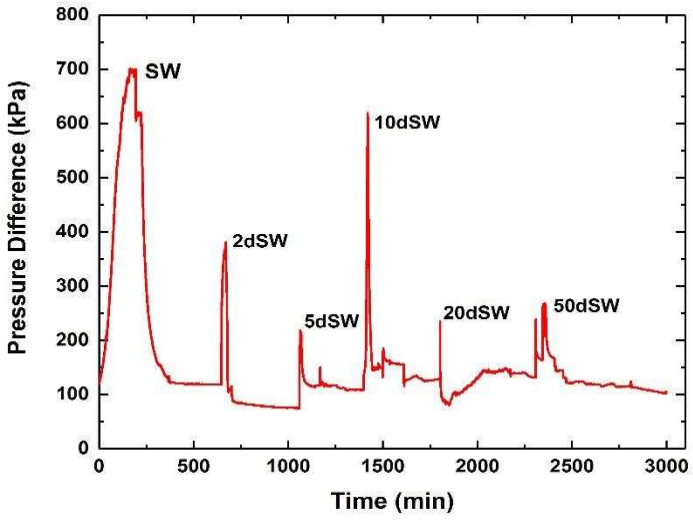

Figure 5. Pressure drop across the hydrophilic micromodel saturated with crude oil A during secondary and tertiary flooding.

It is important to emphasize that during secondary imbibition oil was transported along the pore-throat pairs due to the multiple snap-off and coalescence process, i.e. the flow was under ganglion dynamic regime. It has been reported that the stability of displacement and fluids distribution are controlled by the capillary number (which is defined as $Nc = \nu\mu/\gamma$, where v is the velocity of the injecting fluid, μ is the viscosity of the injecting fluid, and γ is the oil/brine interfacial tension, 31.8 mN/m for seawater) and viscosity ratio (M = μ_w/μ_o, μ_w and μ_o represent the viscosities of the displacing and displaced fluids, respectively) [44]. In the case of seawater injection, the capillary number is low (4.9×10^{-8}) and M <1, indicating that the flow pattern falls within the unstable capillary fingering regime according to Lenormand's stability diagram [45]. The ganglion dynamics happen when oil trapped inside the pore-throat pairs is dominated by capillary forces rather than viscous forces [46,47]. Figure 6 shows two series of magnified images taken at two different locations of the hydrophilic micromodel during secondary seawater imbibition, clarifying snap-off and coalescence events. It is obvious that the snap-off occurred because of water film swelling in a throat between two contiguous pores (marked by a black stippled circle in Fig. 6C). This affects the stability of the oil/brine interface at the throat, leading to a discontinuity in the oil phase and forming an isolated cluster (ganglion), which was finally stabilized in a single pore (Fig. 6D). These observations are in agreement with earlier visual studies by Amirian et al. [34] and Rücker et al. [47] for water-wet systems.

At the beginning of brine flooding, the snap-off process occurred frequently due to the capillary disequilibrium and therefore the number of disconnected oil clusters was increased. After snap-off, the local capillary pressure was relatively increased as the individual clusters tend to find a new place with the minimum local energy [48]. For this, it is observed that the disconnected clusters prefer to internally reconnect (coalesce) with other movable clusters in the adjacent pore with lower capillary pressure, moving then along rigorously from pore-to-pore, leading to an improvement in the microscopic displacement efficiency and a decrease in the oil saturation. This suggested that the viscous forces showed a very small effect on the pore-scale displacement when the high salinity solution was injected, and the

net oil transport was almost due to the ganglion dynamic regime (oil cluster mobilization) even though the associated capillary number is very low (<< 10^{-5}). Figure 6E-G illustrates a sequence of coalescence during seawater injection. As the oil saturation was reduced, the coalesced clusters were trapped into pore throats, and the seawater had continuously proceeded in tandem along the walls of the pore without sweeping the receding oil in the pores' center; hence no more oil was produced after 9 hours of continual seawater flooding.

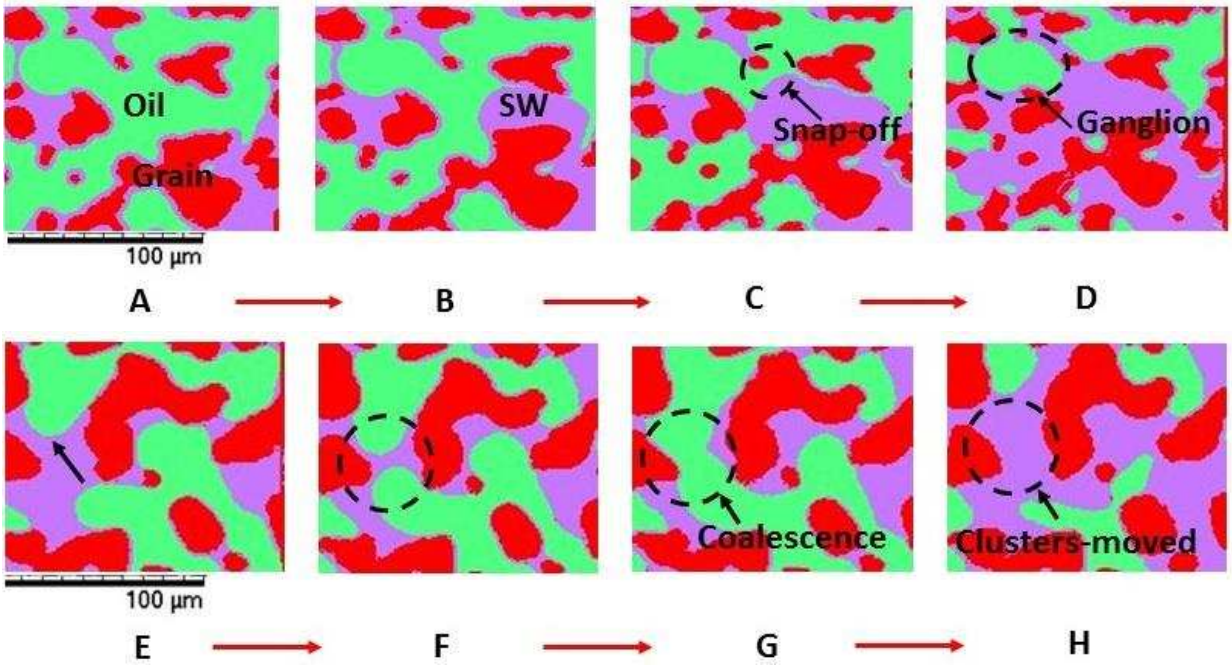

Figure 6: Two series of the same magnified sections at two different locations in the pore network during oil-seawater displacement. (A-D) Shows the sequence of snap-off. (E-H) Shows the sequence of coalescence and ganglia movement. Red: grains, green: oil, purple: brine.

It is obvious that a reduction in the trapped oil clusters was observed in some parts of the network after continuous injection of twice-diluted seawater in tertiary mode (Fig. 4C), resulting in an enhancement in oil recovery of 7% compared to 10% for the case of the micromodel saturated with crude oil B (see Table 3), coinciding with a small reduction in the overall pressure drop, suggesting a

decrease in the flow resistance to brine. The experiments were repeated, and the same trend was observed. It has been reported that the capillary trapping is mostly dominated by the change in the flooding velocity, pore geometry, and rock-fluid interaction (wettability alteration) [33,45,49,50]. In this case, twice diluted seawater was injected at the same low rate as seawater (5 µl/hr); therefore, we expect that the mobilization of oil clusters would not be by viscous forces. Also, a close examination of the pore network images after exposure to twice diluted seawater showed a very minor change in the in-situ contact angle over the time scale of injection, but the wetting state remains within the same strongly water-wet condition, Fig.7B. Such results are incongruent with what was previously observed from some core floods within a Darcy-scale that a reduction in the residual oil saturation with the decrease in brine salinity was attributed to the wettability alteration from strongly water-wet toward an intermediate-wetness [51,52]. However, the findings of the present work agree with the results by other researchers [16], showing higher oil recovery with water-wet wettability. On the other hand, it was found that the interfacial tension was approximately constant (30.5 and 33.7mN/m for oils A and B, respectively) as the seawater was diluted twice from its original concentration. Consequently, the capillary number remains within the low range ($4.6\text{-}5\times10^{-8}$), which is far smaller than that required for residual oil mobilization ($Nc=10^{-5}$ for hydrophilic surface) [25,53].

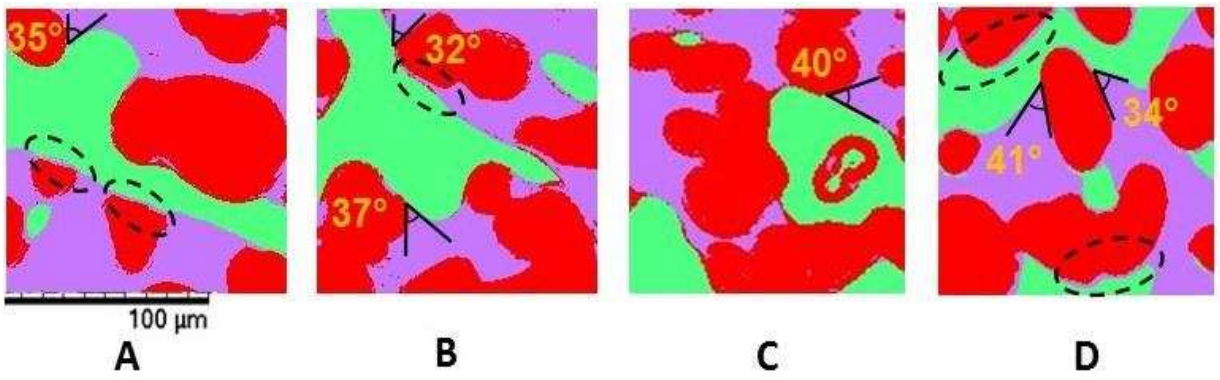

Figure 7. Magnified images at different locations in the hydrophilic micromodel show a typical example for in-situ contact angle between the oil-brine and brine-solid when the system was flushed with (A) seawater, (B) 2dSW, (C) 5dSW and (D) 10dSW. The stippled circles refer to a thin film of brine coated the walls of the pore, preventing oil from reaching the surfaces. Red: grains, green: oil, purple: brine. Resolution of the images= 1.5 µm.

As twice diluted seawater showed less impact on the interfacial properties and therefore on the capillary forces, we found that the most likely reason behind oil mobilization is the reduction in the attractive electrostatic forces (adhesive forces) between the trapped oil and silicate surface. It has been reported that in the presence of a water film the oil/solid interface becomes charged [54]. Furthermore, the low-salinity solution has a neutral pH =7.58 (Table 1), meaning that the silica/brine interface is almost negatively charged [17,37,55]. In comparison with other diluted brines, twice-diluted seawater contained a high concentration of monovalent cations such as Na^+, which could substitute the divalent cations (Ca^{2+} and Mg^{2+}) bonded to the negatively charged polar organic components of oil (-COOH) during secondary seawater injection [17,38]. Thereby, the divalent ions leave the silica surface along with the crude oil, helping to improve the microscopic sweep efficiency. Figure 8 shows the potential chemical interactions between silica/oil/brine at a molecular scale level. The results are qualitatively supported by

our previous work to evaluate the desorption efficiency of oil with different compositions from silica surfaces upon exposure to low saline solutions [38].

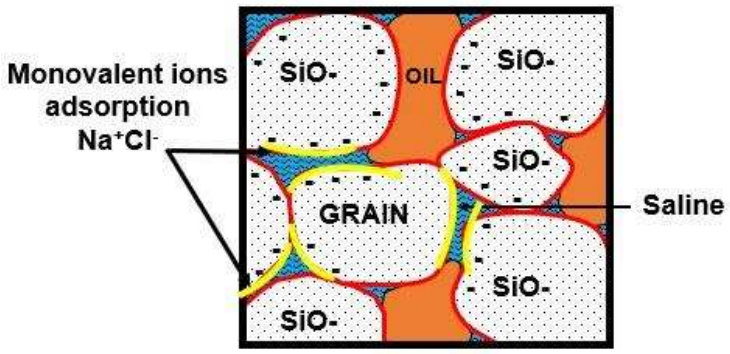

Figure 8. Proposed chemical interactions between oil/brine/hydrophilic surfaces at a molecular scale level.

Another probable explanation in which twice-diluted seawater influences the trapped oil mobilization is by considering the effect of the viscoelastic interface. It has been recently suggested that when the low saline solutions come in contact with the polar organic components of oil, a highly viscoelastic film will be formed [56,57]. It has also been hypothesized that the interactions between the charged surface and the ions in electrolyte will lead to creating an ionic structure along the interface, known as the electrical double layer (EDL) [34,58,59]. The concentration and type of ions existing in the electrolyte play a crucial role in the magnitude of the conductivity and thickness of the electrical double layer. At very high salinity and ionic strength, a shrinkage in the thickness of the EDL would occur and vice versa [60-62]. It is, therefore, speculated that when twice-diluted seawater was flooded continuously for more than 6 hours, an expansion in the electrical double layer (EDL) would happen. This leads to screening off all the interactions with the bulk solution, and hence increasing the affinity of polar organic components into the oil/brine interface, which favorably promoted the viscoelasticity at the interface. As a result, the trapped oil clusters were dispersed in the saline solution, i.e., the sweeping process can be much easier.

Injecting 5dSW into the hydrophilic porous media displayed a minor increase (1% of OOIP) in oil recovery for the micromodel saturated with oil A (see Fig. 4D) but with no improvement in recovery factor for the case of oil B. Any further decrease in the salinity also did not show an increase in the microscopic displacement efficiency for the two kinds of crude oils examined, a typical example is shown in Figure 4E, F. Such results could be traced back to the reduction in the concentration of monovalent ions (Na^+) and therefore their binding at the solid-water interface could be reduced. The EDL expansion could also be not large enough to stimulate the attraction of polar components toward the interface to form the viscoelastic interface. The previous study suggested that a critical expansion of the EDL is required for oil displacement [63]. These results also substantiate previous macroscopic core flooding experiments discussed in the literature that the low-salinity effect on EOR from sandstone (silica) is mostly dominated by the presence of significant clay minerals [64]. The pressure drop was relatively constant with the stepwise low-salinity injection, consistent with a constant resistance to the flow of brine.

3.2 Effect of salinity on the pore-scale displacement efficiency in a hydrophobic network

From the second set of microfluidic experiments, examining the impact of different saline solutions on the microscopic sweeping efficiency in a hydrophobic microstructure, it was found that the initial oil saturation at the end of drainage displacement were 0.87 and 0.84 for oils A and B, respectively. More than half of the oil was trapped in the hydrophobic pore network at the end of secondary flooding by seawater, as the sweeping efficiency were calculated to be 42.5% and 44% for oils A and B, respectively. Repeating the visual experiments with seawater as the displacing fluid results in almost the same recovery factor with the variation of about 2% for the two types of crude oil examined. Figure 9 shows an indicative example of the binary analysis of the micromodel images for a hydrophobic pore network saturated with crude oil A. Like the hydrophilic microstructure, the

corresponding pressure profile at the beginning of seawater flooding was increased, and then it was decreased once the brine displacement front began to cross-flow through the micromodel (Figure 10). It is worth noting that the snap-off-coalescence phenomenon was not observed when brine was flooded through the hydrophobic pore network and brine smoothly displaced oil in a piston-like way with a stable or sometimes irregular displacement front, as the oil was moved ahead of the brine, and only the irreducible oil was left behind the displacement front. Figure 11 shows a typical example of the brine front, advancing with time on the right-hand side of the micromodel.

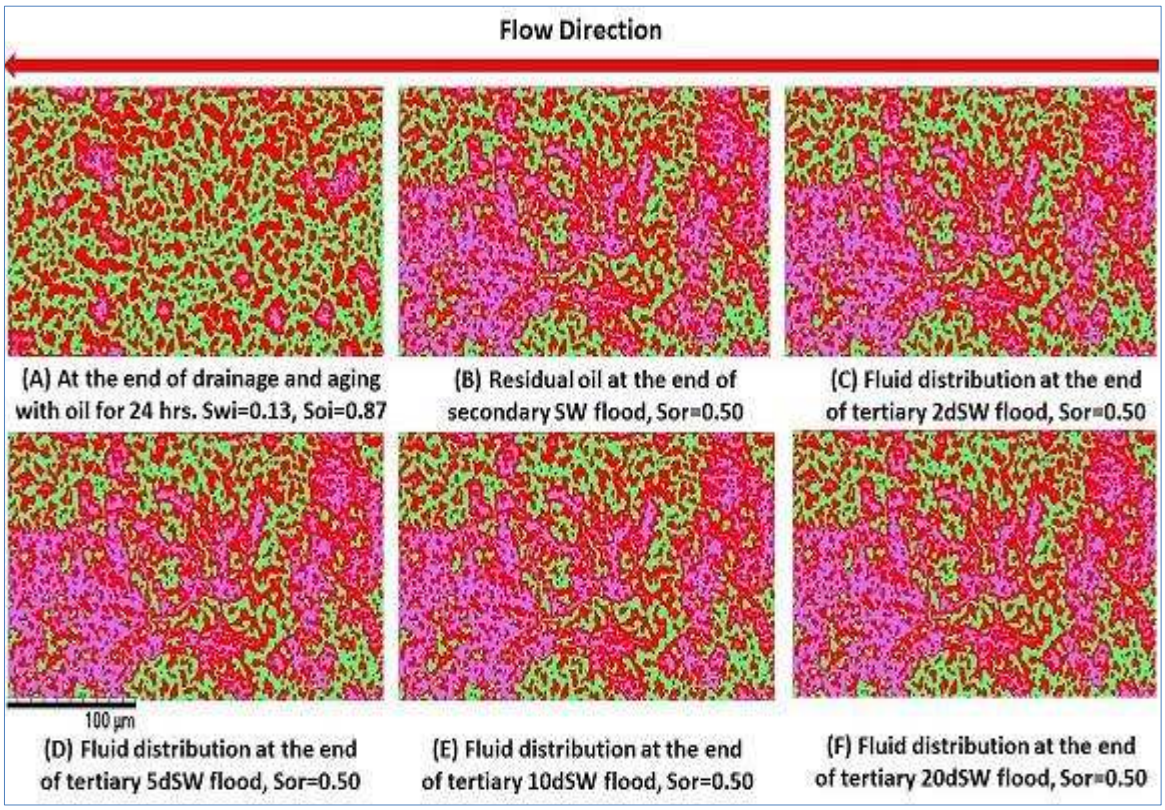

Figure 9. Segmented micromodel images after secondary and tertiary flooding in a hydrophobic surface saturated with crude oil A. Red: grains, green: oil, purple: brine.

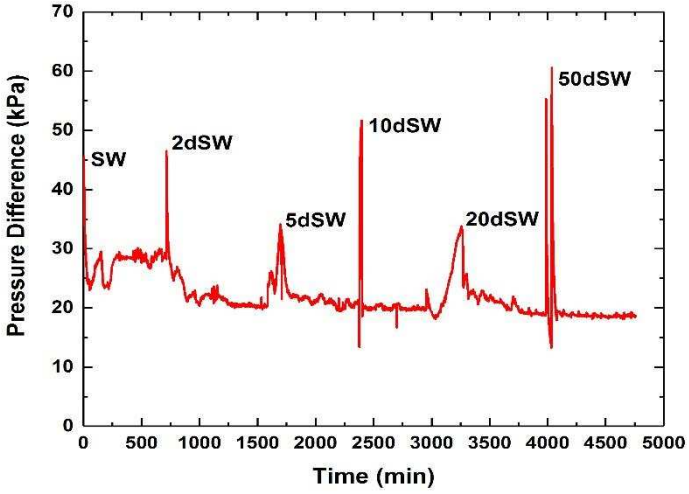

Figure 10. Pressure drop across the hydrophobic micromodel during secondary and tertiary flooding.

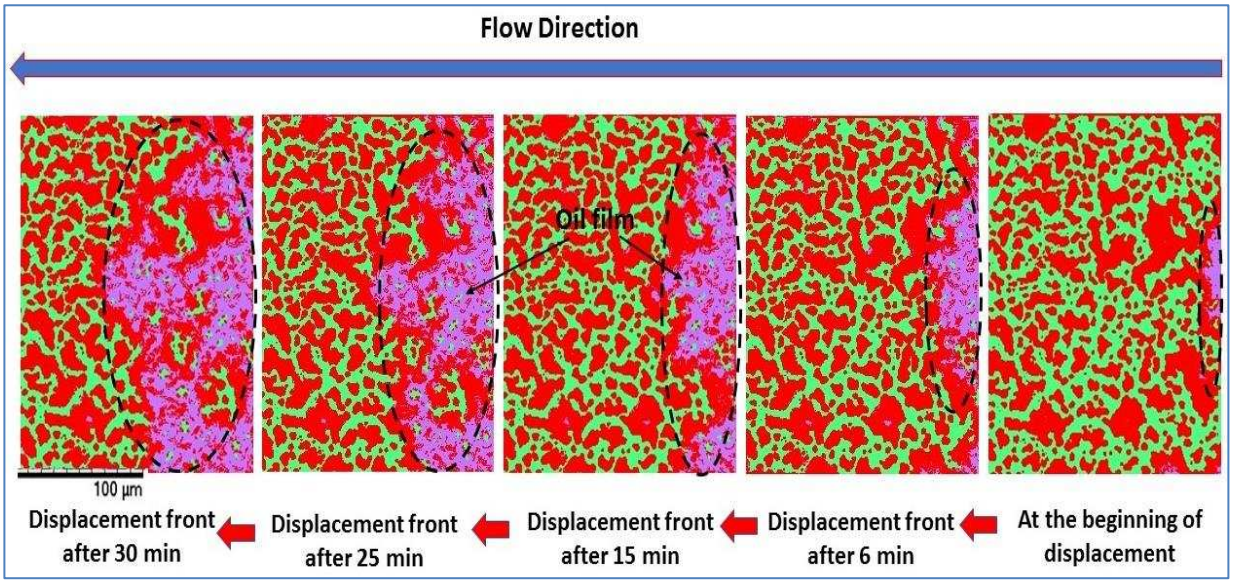

Figure 11. Segmented images, showing brine front advancing during secondary injection in the hydrophobic micromodel. Red: grains, green: oil, purple: brine.

The analysis of recorded images did not show any dramatic change in the residual oil saturation during the sequential flooding of different dilution versions of

seawater, Figure 9C-F, and thereby no positive effect on the microscopic sweeping efficiency. The results also revealed that injecting twice diluted seawater in the hydrophobic micromodel saturated with crude oil B showed a minor improvement (1%) in oil recovery (Table 3). Although the results contradict some macroscopic core flooding experiments that show a positive effect of low salinity on EOR from carbonate surfaces as a result of wettability alteration to preferentially water-wet conditions [10,65], they are in agreement with those of Lager et al. [1] and Fathi et al. [9]. The foremost reason for this inconsistency is due to the fact that in this study the wetting state at the pore scale level did not change during the entire course of low-salinity displacement and all the pore walls remain within a strongly oil-wet condition. Figure 12 illustrates the contact angle and oil/brine interfaces at typical locations at the end of the imbibition displacement. It has been reported that it is difficult to detach polar oil components that bond strongly to the hydrophobic surface by low-salinity solution and the only way to remove them is by increasing the salinity of the injected water, which can promote the reactivity of the surface and modify the wettability to water-wetness [1]. Such a hypothesis is consistent with what is observed in this study during the microscopic displacement. A close inspection of the recorded images in Figure 13 illustrates that a thin oil film coated the walls of the pore that were already invaded by brines, meaning that the surface had a higher affinity to oil than water and therefore promoting the interaction between oil components and grain surfaces. For this, streaming brine toward the grains was not able to replace the attached oil film, and the grain surfaces remain within oil-wet conditions. This could provide compelling evidence that the multiphase flow of the oil-brine system and in-situ contact angle over a pore-scale with a length of micrometers are different from those reported in the literature within a macroscopic scale level [11,14,66], helping in reliably predicting reservoir performance under low-salinity flooding.

The overall pressure drop (Figure 10) across the pore network also remains within the same level during the stepwise low-salinity injection with a value of 20 kPa ± 2, suggesting a constant flow resistance and stable brine flow.

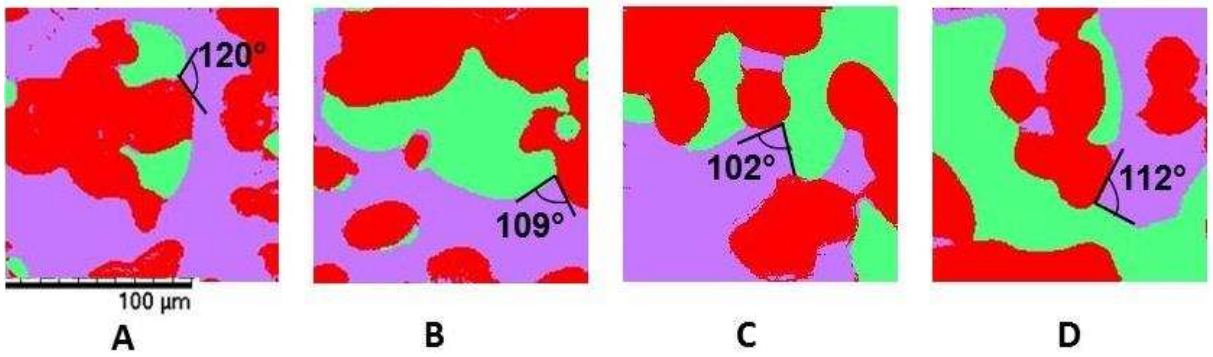

Figure 12. Segmented images of in-situ contact angle measured at different locations in the hydrophobic micromodel when the system was flushed with (A) seawater, (B) 2dSW, (C) 5dSW and (D) 10dSW. Red: grains, green: oil, purple: brine. Resolution of the images = 1.5 µm.

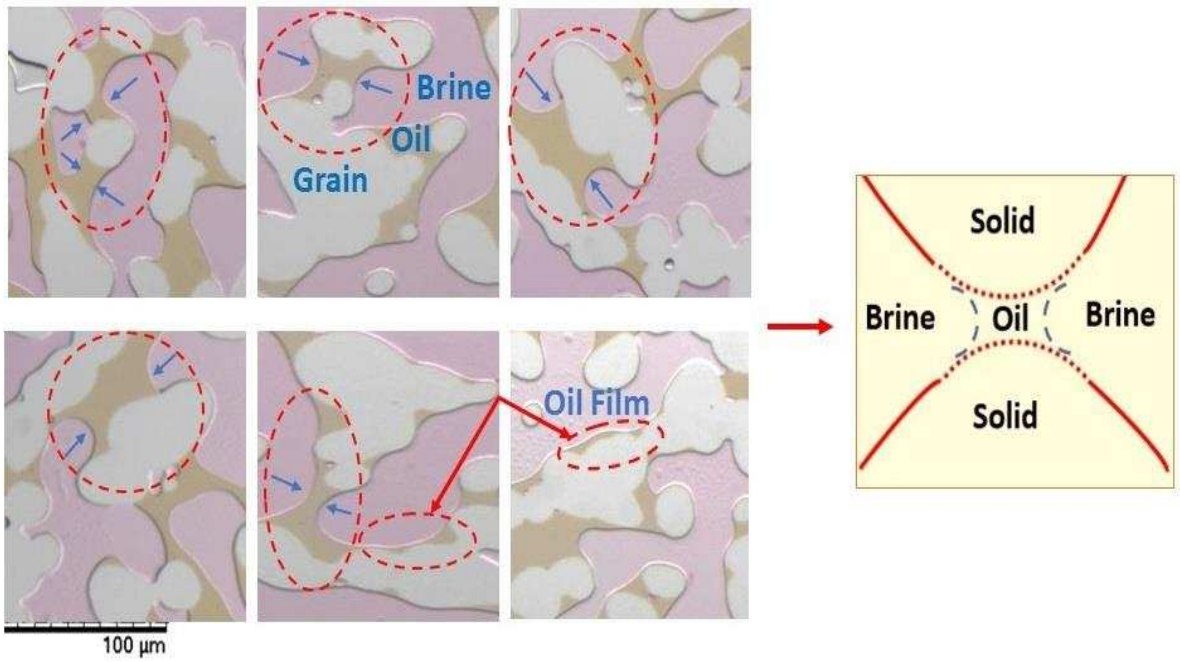

Figure 13. Magnified images at different locations in the hydrophobic micromodel during low-salinity flooding, illustrating strongly oil-wet surfaces as the oil occupies the smallest pores and brine advances over it. Thin oil films are left on the walls of some invaded pores, showing strong adhesive forces between oil and grain surfaces.

3.3 Effect of low salinity flooding on the secondary recovery of the hydrophilic and hydrophobic networks

The other two series of microdisplacement were conducted on hydrophilic and hydrophobic microstructures saturated with crude oil A to examine the efficiency of secondary low-salinity injection on oil production compared to high-salinity solution (seawater). For this, 5 times dilution of seawater was flooded in secondary mode, while 10 times dilution of seawater (4366 ppm) was selected to inject in tertiary mode since previous core flood studies indicated that reducing the salinity of water below 5000 ppm revealed positive results for sandstone and carbonate reservoirs [1-7,10]. Figure 14 shows oil distribution after secondary and tertiary low-salinity flooding through the hydrophilic and hydrophobic pore networks. Obviously, a clear distinction in the magnitude of oil recovery from that of secondary seawater injection was observed (Figure 14A), 49% compared to 57.9% recovered from the seawater secondary flooding under the same test conditions (see Table 3). This might be commonly traced back to the reduction in the ionic strength of the solution, particularly in terms of divalent ion concentration, which was supposed to play the greatest role in the oil desorption efficiency from the water-wet surfaces [67]. However, the discrepancy between high- and low-salinity secondary flooding was less pronounced for a hydrophobic surface. Hence, 38.8% of the oil was produced by injecting 5 times dilution of seawater in secondary mode compared to 42.5 % when seawater was flooded through the hydrophobic surface. Injecting 10 times dilution of seawater in tertiary mode did not reveal any positive effect on the incremental oil recovery for both surfaces examined. This could provide compelling evidence that the sequence of displacement did not heavily affect the potential of low-salinity water to enhance oil recovery, as the same impact of 10 times dilution was observed when high-salinity seawater was injected in secondary mode.

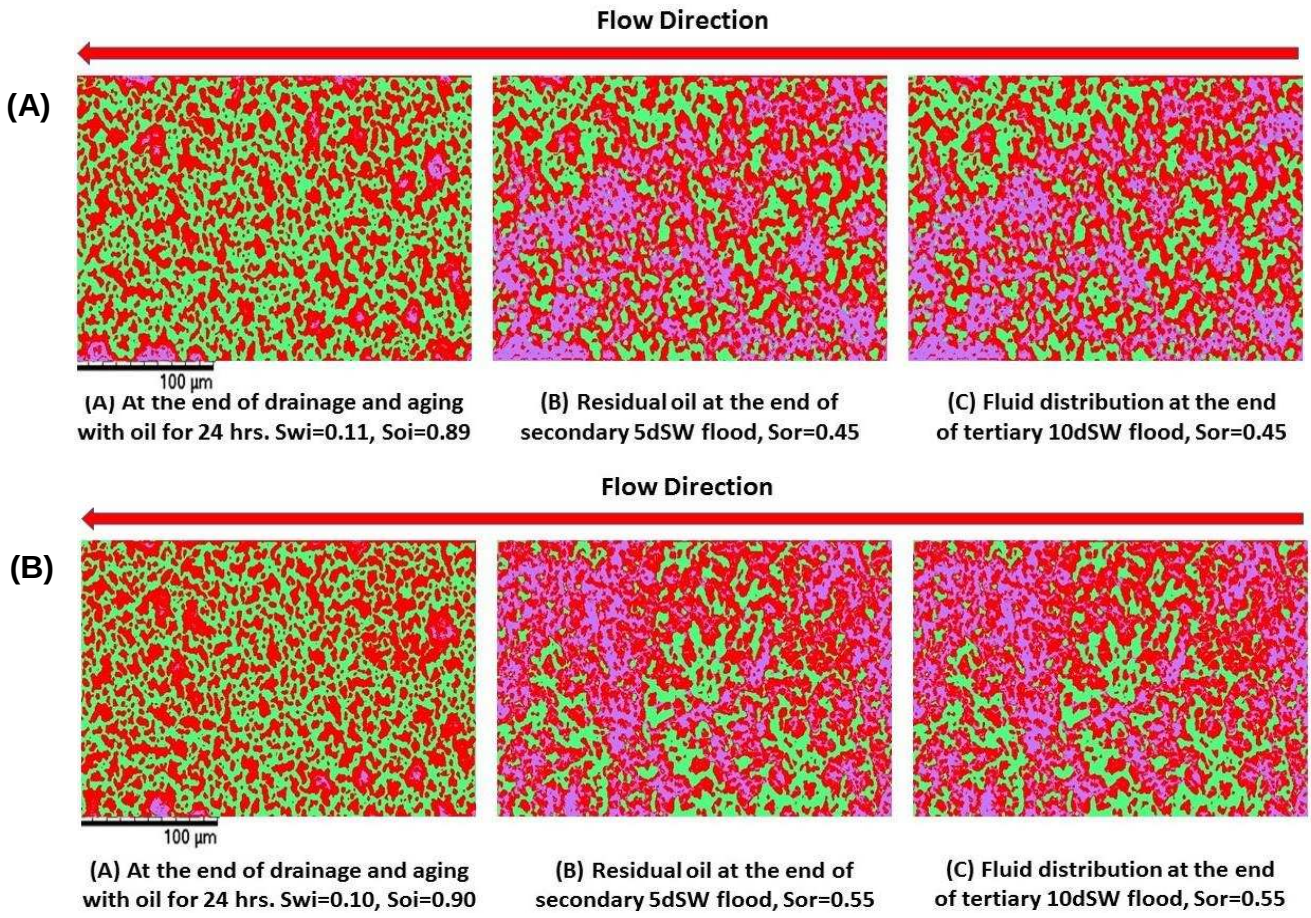

Figure 14. Segmented micromodel images after secondary and tertiary low-salinity flooding for (A) hydrophilic micromodel and (B) hydrophobic micromodel. Red: grains, green: oil, purple: brine.

The overall corresponding pressure drop across the hydrophilic and hydrophobic microstructures recorded during the secondary and tertiary low-salinity water flooding is shown in Figure 15. Peak pressure drops of 93 kPa and 48 kPa were observed before the breakthrough time for the hydrophilic and hydrophobic surfaces, respectively. The pressure was then stabilized at 80 ±3 kPa and 37±2 kPa with the continuous 5 diluted seawater flooding. Injecting 10 times dilution revealed a little further increase in the pressure drop for both surfaces examined with a small fluctuation in the pressure values for the oil-wet microstructure. This could be attributed to the disequilibrium in the local capillary pore pressure and

occasional resistance to flow through the hydrophobic pore network. Such results are in line with what was previously observed from the macroscopic core flooding experiments on chalk, showing higher fluctuations in the pressure drop upon exposure to 10 times dilution [68]. Cissokho et al. [69] also stated that there was an increase in pressure drop when the low-saline solution was injected into the sandstone cores even if no extra oil was recovered.

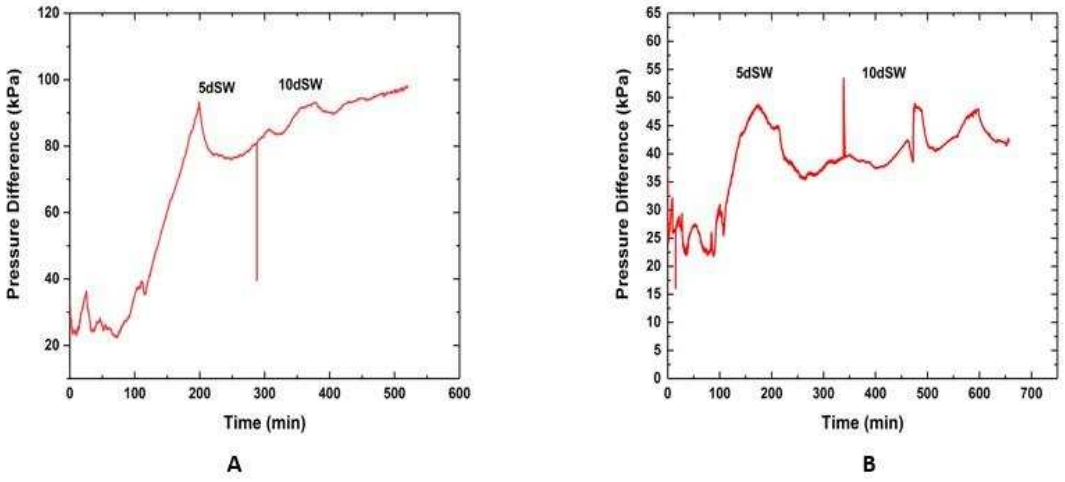

Figure 15. Pressure drop for (A) hydrophilic micromodel. (B) Hydrophobic micromodel during secondary and tertiary low-salinity flooding.

4. Conclusions

In this work, the impact of ionic strength and brine salinity on the pore-scale displacement efficiency is experimentally investigated using two types of micromodel with the same pore geometries but different wetting properties. The results revealed that the dynamics of displacement and flow pattern during secondary flooding by seawater (high salinity) were different in the hydrophilic and hydrophobic surfaces. For the hydrophilic system, oil moved through a multiple

snap-off and coalescence process, while a piston-like displacement of oil by brine was dominant in the oil-wet microstructure. For the hydrophobic microstructure, it was found that no change in the initial wettability was observed during a sequential low-salinity injection as the pore surfaces remain within a strongly oil-wet condition due to the highly bonding effect between polar oil components and pore surfaces. Thereby, tertiary low salinity flooding did not show any positive effect on the microscopic displacement efficiency for the oil-wet system. However, an improvement in oil recovery of 7-10% was observed by injecting twice-diluted seawater through a hydrophilic micromodel due to a reduction in the electrostatic attractive forces (i.e., adhesive forces) and electrical double-layer expansion, which could promote the viscoelasticity at the interface. Furthermore, the effect of oil composition represented by active polar components on the microscopic displacement efficiency is more pronounced for the hydrophilic surface than that of hydrophobic one at different salinities. The potential of low salinity to enhance oil recovery was not affected by the sequence of flooding.

The present findings provide direct evidence that the multiphase flow of the oil/brine system and in-situ contact angle variation at the pore-scale are different from some of those reported previously at the macroscopic scale for both oil-wet and water-wet porous media, suggesting extra cautions are needed to predict and/or interpret the effect of low-salinity injection on reservoir performance.

ACKNOWLEDGMENT

The work is supported by the European Research Council (ERC-2014-CoG, Project reference: 648375) and BP Ltd.

References

1. Lager, A., Webb, K.J., & Collins, I.R. (2008a, January). LoSal Enhanced Oil Recovery: Evidence of Enhanced Oil Recovery at the Reservoir Scale. In SPE Symposium on Improved Oil Recovery. Society of Petroleum Engineers.

2. McGuire, P.L., Chatham, J.R., & Paskvan, F.K. (2005, January). Low Salinity Oil Recovery: An Exciting New EOR Opportunity for Alaska's North Slope. In SPE Western Regional Meeting. Society of Petroleum Engineers.

3. Morrow, N., & Buckley, J. (2011). Improved Oil Recovery by Low-Salinity Water Flooding. Journal of Petroleum Technology, 63 (5), 106-112.

4. Nasralla, R.A., Bataweel, M.A., & Nasr-El-Din, H.A. (2011, September). Investigation of Wettability Alteration by Low Salinity Water. In Offshore Europe. Society of Petroleum Engineers.

5. Seccombe, J., Lager, A., Jerauld, G., Jhaveri, B., Buikema, T., Bassler, S., Denis, J., Webb, K.J., Cockin, A., & Fueg, E. (2010, April). Demonstration of Low-salinity EOR at Inter Well-Scale, Endicott Field, Alaska. In SPE Improved Oil Recovery Symposium. Society of Petroleum Engineers.

6. Vledder, P., Fonseca, J.C., Wells, T., Gonzalez, I.E., & Ligthelm, D.J. (2010, April). Low Salinity Water Flooding: Proof of Wettability Alteration on a Field Wide Scale. In SPE Improved Oil Recovery Symposium. Society of Petroleum Engineers.

7. Webb, K.J., Black, C.J.J., & Al-Ajeel, H. (2004, April). Low Salinity Oil Recovery Log-Inject-Log. In Middle East Oil Show. Society of Petroleum Engineers.

8. Xie, Q., Liu, Y., Wu, J., & Liu, Q. (2014). Ions Tuning Water Flooding Experiments and Interpretation by Thermodynamics of Wettability. Journal of Petroleum Science and Engineering,124, 350-358.

9. Fathi, S.J., Austad, T., & Strand, S. (2010). "Smart Water" as a Wettability Modifier in Chalk: The Effect of Salinity and Ionic Composition. Energy & Fuels, 24 (4), 2514-2519.

10. Yousef, A.A., Al-Saleh, S.H., Al-Kaabi, A., & Al-Jawfi, M.S. (2011). Laboratory Investigation of Injection-Water Salinity and Ionic Content on Oil Recovery from Carbonate Reservoirs. Society of Petroleum Engineers,14 (5), 578-593.

11. Austad, T., Shariatpanahi, S.F., Strand, S., Black, C.J.J., & Webb, K.J. (2012). Conditions for a Low-Salinity Enhanced Oil Recovery (EOR) Effect in Carbonate Oil Reservoirs. Energy & Fuels, 26 (1), 569-575.

12. Austad, T., Shariatpanahi, S.F., Strand, S., Aksulu, H., & Puntervold, T. (2015). Low Salinity EOR Effects in Limestone Reservoir Cores Containing Anhydrite: A Discussion of the Chemical Mechanism. Energy & Fuels, 29 (11), 6903-6911.

13. Strand, S., Hognesen, E.J., & Austad, T. (2006). Wettability Alteration of Carbonates: Effects of Potential Determining Ions (Ca^{2+} and SO_4^{2-}) and Temperature. Colloids and Surfaces A: Physicochemical and Engineering Aspects, 275 (1-3), 1-10.

14. Zhang, P., Tweheyo, M.T., & Austad, T. (2006). Wettability Alteration and Improved Oil Recovery in Chalk: The Effect of Calcium in the Presence of Sulfate. Energy & Fuels, 20 (5), 2056-2062.

15. Zhang, Y., Xie, X., & Morrow, N.R. (2007, November). Water Flooding Performance by Injection of Brine with Different Salinity for Reservoir Cores. In SPE Annual Conference and Exhibition. Society of Petroleum Engineers.

16. Zhang, Y., & Morrow, N.R. (2006, April). Comparison of Secondary and Tertiary Recovery with Change in Injection Brine Composition for Crude Oil/Sandstone Combinations. In SPE/DOE Symposium on Improved Oil Recovery. Society of Petroleum Engineers.

17. Buckley, J.S., & Liu, Y. (1996). Some Mechanisms of Crude/Brine/Solid Interactions. Journal of Petroleum Science and Engineering, 20 (3-4), 155-160.

18. Alotaibi, M.B., Nasralla, R.A., & Nasr-El-Din, H.A. (2011). Wettability Studies Using Low-Salinity Water in Sandstone Reservoirs. SPE Reservoir Evaluation and Engineering,14 (6), 713-725.

19. Martinez, A.W., Phillips, S.T., Whitesides, G.M., & Carrilho, E. (2009). Diagnostics for the Developing World: Microfluidic Paper-Based Analytical Devices. Analytical chemistry, 82, 3-10.

20. Nilghaz, A., Wicaksono, D.H.B., Gustiono, D., Abdul Majid, F.A., Supriyanto, E., & Rafiq Abdul Kadir, M. (2012). Flexible Microfluidic Cloth-Based Analytical Devices Using a Low-Cost Wax Patterning Technique. Lab on a Chip, 12 (1), 209-218.

21. Sieben, V.J., Stickel, A.J., Obiosa-Maife, C., Rowbotham, J., Memon, A., Hamed, N., Ratulowski, J., & Mostowfi, F. (2017). Optical Measurement of Saturates, Aromatics, Resins, and Asphaltenes in Crude Oil. Energy & Fuels, 31(4), 3684-3697.

22. Lin, Y.J., Perrard, A., Biswal, S.L., Hill, R.M., & Trabelsi, S. (2018). Microfluidic Investigation of Asphaltenes-Stabilized Water-in-Oil Emulsions. Energy & Fuels, 32 (4), 4903-4910.

23. Dudek, M., & Øye, G. (2018). Microfluidic Study on the Attachment of Crude Oil Droplets to Gas Bubbles. Energy & Fuels, 32 (10), 10513-10521.

24. Joseph, J., Gunda, N.S.K., & Mitra, S.K. (2013). On-Chip Porous Media: Porosity and Permeability Measurements. Chemical Engineering Science, 99, 274-283.

25. Xu, W., Ok, J.T., Xiao, F., Neeves, K.B., & Yin, X. (2014). Effect of Pore Geometry and Interfacial Tension on Water-Oil Displacement Efficiency in Oil-Wet Microfluidic Porous Media Analogs. Physics of Fluids, 26 (9), 093102.

26. Nilsson, M.A., Kulkarni, R., Gerberich, L., Hammond, R., Singh, R., Baumhoff, E., & Rothstein, J.P. (2013). Effect of Fluid Rheology on Enhanced Oil Recovery in a Microfluidic Sandstone Device. Journal of Non-Newtonian Fluid Mechanics, 202,112-119.

27. Bora, R., Chakma, A., & Maini, B.B. (2003, October). Experimental Investigation of Foamy Oil Flow Using a High Pressure Etched Glass Micromodel. In SPE Annual Technical Conference and Exhibition. Society of Petroleum Engineers.

28. Conn, C.A., Ma, K., Hirasaki, G.J., & Biswal, S.L. (2014). Visualizing Oil Displacement with Foam in a Microfluidic Device with Permeability Contrast. Lab on a Chip,14 (20), 3968-3977.

29. Xu, K., Zhu, P., Colon, T., Huh, C., & Balhoff, M. (2016, April). A Microfluidic Investigation of the Synergistic Effect of Nanoparticles and Surfactants in Macro-Emulsion Based EOR. In SPE Improved Oil Recovery Conference. Society of Petroleum Engineers.

30. Lacey, M., Hollis, C., Oostrom, M., & Shokri, N. (2017). Effects of Pore and Grain Size on Water and Polymer Flooding in Micromodels. Energy & Fuels, 31(9), 9026-9034.

31. Xu, K., Agrawal, D., & Darugar, Q. (2018). Hydrophilic Nanoparticle-Based Enhanced Oil Recovery: Microfluidic Investigations on Mechanisms. Energy & Fuels, 32 (11), 11243-11252.

32. Emadi, A., & Sohrabi, M. (2013, September). Visual Investigation of Oil Recovery by Low Salinity Water Injection: Formation of Water Micro-

Dispersions and Wettability Alteration. In SPE Annual Technical Conference and Exhibition. Society of Petroleum Engineers.

33. Barnaji, M.J., Pourafshary, P., & Rasaie, M.R. (2016). Visual Investigation of the Effects of Clay Minerals on Enhancement of Oil recovery by Low Salinity Water Flooding. Fuel,184, 826-835.

34. Amirian, T., Haghighi, M., & Mostaghimi, P. (2017). Pore Scale Visualization of Low Salinity Water Flooding as an Enhanced Oil Recovery Method. Energy & Fuels, 31(12), 13133-13143.

35. Fredriksen, S.B., Rognmo, A.U., & Fernø, M.A. (2018). Pore-Scale Mechanisms during Low Salinity Water flooding: Oil Mobilization by Diffusion and Osmosis. Journal of Petroleum Science and Engineering,163, 650-660.

36. Klemme, H.D., & Ulmishek, G.F. (1991). Effective Petroleum Source Rocks of the World: Stratigraphic Distribution and Controlling Depositional Factors (1). AAPG Bulletin, 75 (12), 1809-1851.

37. Anderson, W.G. (1986). Wettability Literature Survey-Part 1: Rock/Oil/Brine Interactions and the Effects of Core Handling on Wettability. Society of Petroleum Engineer, 38 (10), 1125-1127.

38. Al-Khafaji, A., Neville, A., Wilson, M., & Wen, D. (2017). Effect of Low Salinity on the Oil Desorption Efficiency from Calcite and Silica Surfaces. Energy & Fuels, 31(11),11892-11901.

39. Fulcher Jr, R.A., Ertekin, T., & Stahl, C.D. (1985). Effect of Capillary Number and Its Constituents on Two-Phase Relative Permeability Curves. Journal of Petroleum Technology, 37(2), 249-260.

40. Speight, J.G. (2006). Chemistry and Technology of Petroleum. 4th Ed. Hoboken: Taylor and Francis.

41. Meredith, W., Kelland, S.J., & Jones, D.M. (2000). Influence of biodegradation on crude oil acidity and carboxylic acid composition. Organic Geochemistry, 31(11), 1059-1073.

42. Barth, T., Høiland, S., Fotland, P., Askvik, K.M., Pedersen, B.S., & Borgund, A. E. (2004). Acidic compounds in biodegraded petroleum. Organic geochemistry, 35 (11-12), 1513-1525.

43. Farooq, U., Sjøblom, J., & Øye, G. (2011). Desorption of Asphaltenes from Silica-Coated Quartz Crystal Surfaces in Low Saline Aqueous Solutions. Journal of Dispersion Science and Technology, 32 (10), 1388-1395.

44. Avraam, D.G., & Payatakes, A.C. (1995). Flow Regimes and Relative Permeabilities during Steady-State Two-Phase Flow in Porous Media. Journal of Fluid Mechanics, 293, 207-236.

45. Lenormand, R., Touboul, E., & Zarcone, C. (1988). Numerical Models and Experiments on Immiscible Displacements in Porous Media. Journal of Fluid Mechanics,189,165-187.

46. Murison, J., Semin, B., Baret, J.-C., Herminghaus, S., Schröter, M., & Brinkmann, M. (2014). Wetting Heterogeneities in Porous Media Control Flow Dissipation. Physical Review Applied, 1642 (3), 034002.

47. Rücker, M., Berg, S., Armstrong, R.T., Georgiadis, A., Ott, H., Schwing, A., Neiteler, R., Brussee, N., Makurat, A., Leu, L., Wolf, M., Khan, F., Enzmann, F., & Kersten, M. (2015). From Connected Pathway Flow to Ganglion Dynamics. Geophysical Research Letters, 42 (10), 3888-3894.

48. Singh, K., Menke, H., Andrew, M., Lin, Q., Rau, C., Blunt, M.J., & Bijeljic, B. (2017). Dynamics of Snap-off and Pore-Filling Events during Two-Phase Fluid Flow in Permeable Media. Scientific Reports, 7(1), 5192.

49. Moore, T.F., & Slobod, R.L. (1955, October). Displacement of Oil by Water-Effect of Wettability, Rate, and Viscosity on Recovery. In Meeting of the Petroleum Branch of AIME. Society of Petroleum Engineers.

50. Zheng, X., Mahabadi, N., Yun, T.S., & Jang, J. (2017). Effect of Capillary and Viscous Force on CO_2 Saturation and Invasion Pattern in the Microfluidic Chip. Journal of Geophysical Research: Solid Earth,122 (3),1634-1647.

51. Agbalaka, C.C., Dandekar, A.Y., Patil, S.L., Khataniar, S., & Hemsath, J.R. (2009). Coreflooding Studies to Evaluate the Impact of Salinity and Wettability on Oil Recovery Efficiency. Transport in Porous Media, 76 (1), 77-94.

52. Al-Attar, H.H., Mahmoud, M.Y., Zekri, A.Y., AlMehaideb, R., & Ghannam, M. (2013). Low –Salinity Flooding in a Selected Carbonate Reservoir: Experimental Approach. Journal of Petroleum Exploration and Production Technology, 3 (2), 139-149.

53. Lake, L.W. (1989). Enhanced Oil Recovery. Upper Saddle River, New Jersey, Prentice Hall.

54. Buckley, J.S., Liu, Y., & Monsterleet, S. (1998). Mechanisms of Wetting Alteration by Crude Oils. Journal of Petroleum Science and Engineering, 3 (1), 54-61.

55. Liu, X., Yan, W., Stenby, E.H., & Thormann, E. (2016). Release of Crude Oil from Silica and Calcium Carbonate Surfaces: On the Alternation of Surface and Molecular Forces by High-and Low-Salinity Aqueous Salt Solutions. Energy & Fuels, 30 (5), 3986-3993.

56. Chávez-Miyauchi, T.E., Firoozabadi, A., & Fuller, G.G. (2016). Nonmonotonic Elasticity of the Crude Oil–Brine Interface in Relation to Improved Oil Recovery. Langmuir, 32 (9), 2192-2198.

57. Morin, B., Liu, Y., Alvarado, V., & Oakey, J. (2016). A Microfluidic Flow Focusing Platform to Screen the Evolution of Crude Oil–Brine Interfacial Elasticity. Lab on a Chip,16 (16), 3074-3081.

58. Derjaguin, B., & Landau, L. (1993). Theory of the Stability of Strongly Charged Lyophobic Sols and of the Adhesion of Strongly Charged Particles in Solutions of Electrolytes. Progress in Surface Science, 43 (1), 30-59.

59. Overbeek, J.T.G., & Verwey, E. (1948). Theory of the Stability of Lyophobic Colloids: The Interaction of Sol Particles Having an Electric Double layer. Mineola, New York, USA: Dover Publication Inc.

60. Dishon, M., Zohar, O., & Sivan, U. (2009). From Repulsion to Attraction and Back to Repulsion: The Effect of NaCl, KCl, and CsCl on the Force between Silica Surfaces in Aqueous Solution. Langmuir, 25 (5), 2831-2836.

61. Hilner, E., Andersson, M.P., Hassenkam, T., Matthiesen, J., Salino, P.A., & Stipp, S.L.S. (2015). The Effect of Ionic Strength on Oil Adhesion in Sandstone - The Search for the low Salinity Mechanism. Scientific Reports, 5, 9933.

62. Mugele, F., Siretanu, I., Kumar, N., Bera, B., Wang, L., de Ruiter, R., Maestro, A., Duits, M., van den Ende, D., & Collins, I. (2016). Insights from Ion Adsorption and Contact-Angle Alteration at Mineral Surfaces for Low-Salinity Waterflooding. SPE Journal, 21 (04), 1203-1213.

63. Farooq, U., Asif, N., Tweheyo, M.T., Sjöblom , J., & Øye, G. (2011). Effect of Low-Saline Aqueous Solutions and pH on the Desorption of Crude Oil Fractions from Silica Surfaces. Energy & Fuels, 25 (5), 2058-2064.

64. Tang, G.O., & Morrow, N.R. (1999). Influence of Brine Composition and Fines Migration on Crude Oil/Rock Interactions and Oil Recovery. Journal of Petroleum Science and Engineering, 24 (2-4), 99-111.

65. Yi, Z., & Sarma, H.K. (2012, November). Improving Water flood Recovery Efficiency in Carbonate Reservoirs through Salinity Variations and Ionic Exchanges: A Promising Low-Cost "Smart-Water flood" Approach. In Abu Dhabi International Petroleum Conference and Exhibition. Society of Petroleum Engineers.

66. Alshakhs, M.J., & Kovscek, A.R. (2016). Understanding the Role of Brine Ionic Composition on Oil Recovery by Assessment of Wettability from Colloidal Forces. Advances in Colloid and Interface Science, 233,126-138.

67. Lager, A., Webb, K.J., Black, C.J.J., Singleton, M., & Sorbie, K.S. (2008b) Low Salinity Oil Recovery-An Experimental Investigation1. Petrophysics, 49 (1).

68. Hamouda, A.A., & Gupta, S. (2017). Enhancing Oil Recovery from Chalk Reservoirs by a Low-Salinity Water Flooding Mechanism and Fluid/Rock Interactions. Energies,10 (4), 576.

69. Cissokho, M., Bertin, H., Boussour, S., Cordier, P., & Hamon, G. (2010). Low Salinity Oil Recovery on Clayey Sandstone: Experimental Study. Petrophysics, 51(5), 305-313.